Annals of Glaciology

Article

Cite this article: Saltiel S, Groebner N, Sawi T, McCarthy C (2024). Characterization of seismicity from different glacial bed types: machine learning classification of laboratory stick-slip acoustic emissions. *Annals of Glaciology* 1–8. https://doi.org/10.1017/aog.2024.11

Received: 13 December 2023
Revised: 31 January 2024
Accepted: 1 March 2024

Keywords:
Seismicity; subglacial exploration geophysics; subglacial processes; seismology; glacier geophysics

Corresponding author:
Seth Saltiel; Email: ssaltiel@cornell.edu

cambridge.org/aog

Characterization of seismicity from different glacial bed types: machine learning classification of laboratory stick-slip acoustic emissions

Seth Saltiel[1], Nathan Groebner[2], Theresa Sawi[3] and Christine McCarthy[3]

[1]Earth and Atmospheric Sciences, Cornell University, Ithaca, NY, USA; [2]Department of Research, Strabo Analytics, Inc, New York, NY, USA and [3]Lamont-Doherty Earth Observatory, Columbia University of New York, NY, USA

Abstract

Subglacial seismicity presents the opportunity to monitor inaccessible glacial beds at the epicentral location and time. Glaciers can be underlain by rock or till, a first order control on bed mechanics. Velocity-weakening, necessary for unstable slip, has been shown for each bed type, but is much stronger and evolves over more than an order of magnitude longer distances for till beds. Utilizing a destiffened double direct shear apparatus, we found conditions for instability at freezing temperatures and high slip rates for both bed types. During stick–slip stress-drops, we recorded acoustic emissions with piezoelectric transducers frozen into the ice. The two populations of event waveforms appear visually similar and overlap in their statistical features. We implemented a suite of supervised machine learning algorithms to classify the bed type of recorded waveforms and spectra, with prediction accuracy between 65–80%. The Random Forest Classifier is interpretable, showing the importance of initial oscillation peaks and higher frequency energy. Till beds have generally higher friction and resulting stress-drops, with more impulsive first arrivals and more high frequency content compared to rock emissions, but rock beds can produce many till-like events. Seismic signatures could enhance interpretation of bed conditions and mechanics from subglacial seismicity.

1. Introduction

Future sea-level rise will largely be determined by fast-slipping polar glaciers, known as ice streams (Cuffey and Paterson, 2010). Since motion is mostly concentrated at their beds, conditions there have an outsized effect on the entire system's mass-balance and evolution. Glacial beds are commonly separated, to first order, into hard bedrock or soft sediment (till), and then as either 'wet' (melting temperature and undrained) or 'dry' (frozen or drained) (Clarke, 2005). Water and sediment can flow and evolve on much shorter time scales than ice deforms, so the bed is one of the most dynamic parts of the ice sheet system, assumed to be responsible for recent changes in ice flow configurations (Bougamont and others, 2015) and ongoing responses to the changing climate (Parizek and others, 2013).

Although the basal system is difficult to directly access, growing observations of subglacial seismicity offer the opportunity to monitor changes with high temporal and spatial resolution (Aster and Winberry, 2017). Recent studies have used subglacial seismicity observations to infer differences in bed strength (Guerin and others, 2021), failure mechanism (Kufner and others, 2021), fine-scale asperity interactions (Gräff and others, 2021), basal water pressure (Gräff and Walter 2021), local basal shear-stresses and slip-rates (Hudson and others, 2023), and temporal transients in slip tied to fluctuations in meltwater supply (Stevens and others, 2024).

Seismic observations are particularly useful since there are limited glacial bed conditions that have been shown to exhibit the requisite conditions for seismic failure (Iverson, 2010; Lipovsky and others, 2019). Classically, ice deformation, and thus slip due to regelation and viscous creep, is assumed to be rate-strengthening (Weertman, 1957). Till deformation was also first treated as viscous but later shown to be Coulomb plastic, essentially rate-neutral (Iverson, 2010, Zoet and Iverson, 2020). Nucleation of the slip instability that produces seismic waves requires rate-weakening resistance, allowing feedback between accelerating slip and decreasing friction. Earthquake mechanics have long used an empirical formulation to describe the rate dependence of frictional resistance and its evolution with the state of the sliding interface, known as rate-state friction (Dietrich, 1979; Ruina, 1983). Within this formalism, the degree of rate-weakening is given by the amplitude of the positive stability parameter ($b - a$), while rate-strengthening gives a negative value (e.g., Marone, 1998). This friction law has recently been used to model dynamic subglacial drag, such as during stick–slip seismicity (Gräff and Walter, 2021; Hudson and others, 2023), tremor (Lipovsky and Dunham, 2016) and surge behaviors (Thøgersen and others, 2019; Minchew and Meyer, 2020). Stick-slip can also be modeled by a simple decrease in friction from its stuck, static value (f_s) to a kinetic value (f_k) over some slip displacement (d_c) (Sergienko and others, 2009; Goldberg and others, 2014), referred as slip-weakening friction in earthquake modeling (Ida, 1972).

The ability to produce seismic, unstable acceleration, is controlled by the balance between the elastic stiffness (k) of the surrounding material (ice for glaciers or wall rock in the case of

faults), which transmits the driving stress to the interface and the frictional evolution of resistance on the interface, captured by the rheological critical stiffness (k_{cr}), which can be expressed using rate-state friction parameters (Zoet and others, 2020). To build up and release elastic energy with unstable stick–slip cycles, the elastic driving stress must be released more slowly than the frictional resistance decreases during acceleration, as described by the following inequality:

$$k < k_{cr} = \left(\frac{(b-a)\sigma}{D_c}\right), \quad \text{or } k < k_{cr} = \left(\frac{(f_s - f_k)\sigma}{d_c}\right), \qquad (1)$$

where σ is effective normal stress, overburden minus pore pressure, and D_c is the critical slip distance over which friction evolves in the rate-state law; the second relation is for a slip-weakening type friction law. The stiffness control on stability has been demonstrated for fault (e.g., Marone, 1998) as well as glacial bed materials (Zoet and others, 2020). This situation provides the opportunity for seismic observations to present a strong constraint on the conditions at their epicentral location and origin time, but each potential stick–slip mechanism and characteristics of resulting seismicity must be thoroughly understood to determine what conditions recorded seismic events represent.

Laboratory simulations provide the opportunity to directly observe slip behavior under controlled conditions. To date, seismically required rate-weakening has been reported for debris-laden ice on impermeable rock at sub-freezing temperature and permeable rock at the pressure melting point (Zoet and others, 2013), pure ice on impermeable rock at sub-freezing temperature (McCarthy and others, 2017), and pure ice on till at sub-freezing temperature (Saltiel and others, 2021), with stick–slip stress-drops reported for debris-laden ice on impermeable rock at sub-freezing temperature (Zoet and others, 2020). These findings suggest that seismicity is largely associated with dry (frozen or drained) conditions. Although fast-slipping glaciers are commonly assumed to occur on wet, temperate till beds, which have been shown to be velocity strengthening (Lipovsky and others, 2019; Zoet and Iverson, 2020; Saltiel and others, 2021), local mechanisms could freeze bed regions, for example around obstacles (de Robin, 1976). Experiments have also shown rate-weakening is possible due to cavity formation behind hard bed obstacles (Zoet and Iverson, 2016) and pore-pressure feedback from clast plowing (Thomason and Iverson, 2008). Although each of these mechanisms, and the bed conditions which enable them, show rate-weakening drag, their frictional evolution can differ dramatically. For example, the critical slip distance (D_c) over which friction evolves to a new steady-state after a change in slip rate varies by more than an order of magnitude between rock and till beds under similar conditions in the same apparatus (McCarthy and others, 2017; Saltiel and others, 2021). These mechanisms' different frictional mechanics and applicable scales likely contribute to aspects of the resulting seismicity, which could further constrain epicentral bed conditions.

We report here, for the first time, experimental stick–slip stress-drops for pure ice on impermeable rock and till at sub-freezing temperatures. In addition, we measured acoustic emissions (AEs) from these settings and analyze the measured waveforms using machine learning (ML) classification algorithms to find the characteristics associated with each bed type. By improving our understanding of the mechanisms of unstable slip in glacial settings and their expression in seismic emissions, these experiments and analysis techniques provide the opportunity to extract more information on conditions/source mechanics of subglacial or other seismic settings.

2. Experimental methods and materials

Experiments were conducted using an ambient pressure, cryogenic temperature, servo-hydraulic biaxial friction apparatus (McCarthy and others, 2016), with modifications to the insulating cryostat and loading procedure to allow measurement of till (Saltiel and others, 2021). In this double-direct-shear configuration, a central ice block slides against two stationary side blocks, with 10 mm thick layers of pre-compacted and frozen Matanuska till or Barre granite rock on opposite sides of the ice, such that applied horizontal load is resolved as normal stress (horizontal force over the surface area of each side block, 50 mm × 50 mm) and vertical load as shear stress on the two sliding interfaces (vertical force over the surface area of both side blocks, 2 × 50 mm × 50 mm).

As in Saltiel and others (2021), we control temperature with Peltier thermoelectric coolers in front and behind the ice block, as well as circulation of chiller fluid through the side blocks where both temperature and flow rate of chiller fluid were actively controlled to reach and sustain the desired temperature. Resistance Temperature Detectors (RTDs) ported directly behind the till or rock monitor the temperature as close to the sliding interfaces as possible.

In this study, all experiments used ~50 kPa of normal stress with displacement control using a load point velocity of 100 $\mu m\, s^{-m}$ (the slope of the black line on the bottom of Fig. 1b), just over 3 $km\, yr^{-r}$, around the surface velocity of the fastest ice streams (Zoet and others, 2020). Since the load point Linear Variable Differential Transformer (LVDT) only has 20 mm of stroke, the load point was stopped halfway through each experiment and then LVDT was reset to complete the rest of the experimental displacement. In this way, every experiment included a hold of about 60 s during which the shear stress relaxed and then reloaded, usually resulting in the largest stress-drop and AE of each experiment (see Fig. 2). This also provides a measurement of the interface's degree of healing. The cryostat and sample assembly are diagramed in Figure 1a, while additional experimental details are described in supplementary text S1.

We made three additional modifications to the apparatus from Saltiel and others (2021). A Linear Variable Inductance Transducer (LVIT) position sensor measures the sample displacement separate from the loading point's preset displacement. This allowed measurement of displacement in each stress-drop 'slip' event as well as slip occurring during 'stuck' periods and the timing coincident with stress-drops (Fig. 1b). Here we refer only to mechanical or bulk stress-drops, the stress change over a slip event as measured by our vertical load cell, not to be confused with seismologically derived stress-drops. A piece of rubber was inserted into the loading geometry that effectively reduced the stiffness of the apparatus, reaching critical stiffness and allowing stick–slip instability (Zoet and others, 2020). We estimate the effective apparatus stiffness using the mechanical data's reloading slope between stress-drops, relative to the compression of the loading train including rubber, the load point displacement minus sample displacement (Fig. 1b), giving the apparatus stiffness with the rubber to be ~0.1 $kPa\, \mu m^{-1}$, significantly less stiff than was estimated without the rubber ~1 $kPa\, \mu m^{-1}$ (Saltiel and others, 2021). Additionally, commercial piezoelectric transducers were frozen into the central ice block, facing the right ice-bed interface, to measure AEs. The sensor has a directionality, measuring waves incident on the transducer face, but waves could also arrive after bouncing around the sample. Recorded later arrivals (Video 1 in supplement) likely represent reflections from the other interface. We tried four different transducer types of varying size and frequency sensitivity, settling on Physical Acoustic's Nano 30^{TM} miniature AE sensor due to its small size and 125–750 kHz response, covering most of our measured frequency content. All AEs analyzed here were recorded with a single Nano-30.

https://doi.org/10.1017/aog.2024.11 Published online by Cambridge University Press

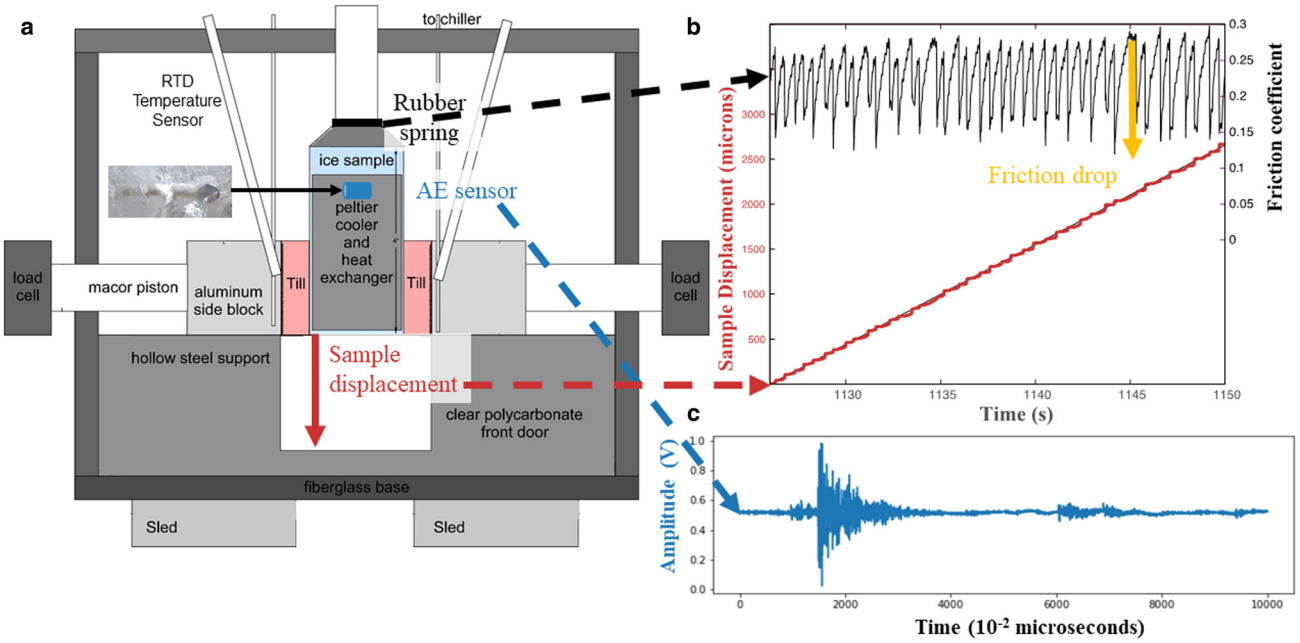

Figure 1. (a) Schematic of biaxial cryostat with additions of rubber spring, to decrease loading stiffness, AE sensor frozen into central ice bock (pictured within ice in inset on left) and sample displacement measurement. For more details about apparatus see Saltiel and others (2021) and supplementary text S1. (b) An example experiment of measured friction drops (in black on top) and stick–slip sample displacement (in red on the bottom) with the steady load point displacement (in black) for reference. Orange arrow shows an example of how friction drop is measured, stress drop is calculated by multiplying friction drop by the constant normal stress of 50 kPa. Instability was induced by apparatus reaching subcritical stiffness (k_{cr}). (c) An example AE waveform before processing, from a single stress-drop.

AEs were recorded using a preamplifier and TiePie^{TM} HS6 differential digital oscilloscope. To ensure we recorded all relevant spectral content in the waveforms, they were recorded at a sample rate of 100 MHz for 1 ms time windows around each event (Fig. 1c). These oscilloscope settings provided the optimal real-time viewing of waveforms as they were being recorded (Video 1 in supplement), but subsequent analysis showed most of the energy was under 1 MHz, and waveforms were down sampled to 10 MHz. Recordings of continuous acoustic signal without applied shear found electrical noise above 3 MHz, so filtering also helped remove persistent noise sources. The oscilloscope was set in rising-limb trigger mode with trigger amplitude set just above the noise level before slip initiates, such that it did not trigger without an audible stress-drop. Since electrical and other sources of noise can vary, this trigger level was adjusted throughout the experiment to maximize the number of captured events and minimize waveforms of purely noise, but some events were missed, and some events triggered by noise or other AE sources were saved.

3. Stick-slip instability at frozen conditions

Both rock and till experiments were undertaken over a range of temperatures, showing the temperature dependence of instability. Analyzing the temperature dependence of AE characteristics is outside of the scope of this article and will be explored in future work. We found stress-drops only at frozen temperatures, < ~0°C for rock and <~−2.5°C for till beds (Fig. 2). It must be noted that temperatures are approximate since they are measured behind the till/rock. This is accurate for stable temperatures, but there is an unknown time lag before the temperature on the sliding interface reaches the recorded temperature. Additionally, when the temperature probe goes above the pressure melting point, ~0°C, the ice will remain at its pressure melting point. The rock or till layer is 10 mm thick and given thermal diffusivities ~1 mm^2 s^{-1}, we estimated the lag time to be ~100 s, given by the yellow region after the recorded temperature in Figure 2. The observed temperature dependent stability is consistent with rate-weakening friction shown for till beds at ~ −3°C, but not at the pressure melting point (Saltiel and others, 2021). We estimate (Eqn (1)) the apparatus stiffness with rubber to be the same order of magnitude as the critical stiffness estimated from separate velocity-step experiments under similar conditions ~0.02 kPa μm^{-1} (Saltiel and others, 2021). The factor of five difference is consistent with the error inherit in applying estimations of rate-state friction parameters ($b - a$, D_c) from a single experiment, as well as in our rough estimation of apparatus stiffness. Past studies of ice on rock friction did not find rate-weakening until lower temperatures, <~−18°C for McCarthy and others (2017). In that study, experiments above −18°C which exhibited slight rate-strengthening were undertaken at less than half the slip rate, which could affect the rate-dependence (Zoet and others, 2013; Saltiel and others, 2021) as well as stability more broadly (Schulson and Fortt, 2012). It is also possible to reach instability at nominally stable conditions given the strong elastic contrast between ice and rock beds (Rice and others, 2001). This highlights the range of factors that contribute to seismic instability, and why further experiments and analysis are needed to fully map the conditional dependence of stability.

4. Data processing and machine learning analysis

Each experiment starts with an elastic loading ramp, after which we observe abrupt and audible stress drop events (Supplementary Video 1 and Figs 1b and 2). Most events directly correspond to bulk mechanical stress drops (see Fig. 1b), but to remove AEs associated with other types of sources (such as smaller patches of slip), noisy events, nonevents triggered by noise, and to normalize the waveforms in a way that focuses on the initial wave arrivals (removing secondary wave arrivals), we implemented a data cleaning and normalization approach based on that implemented by Nolte and Pyrak-Nolte (2022).

First, waveforms were trimmed to a total of 1200 data points, including 400 sample points before the trigger point, giving a total window of 120 microseconds. Waveforms were then normalized

https://doi.org/10.1017/aog.2024.11 Published online by Cambridge University Press

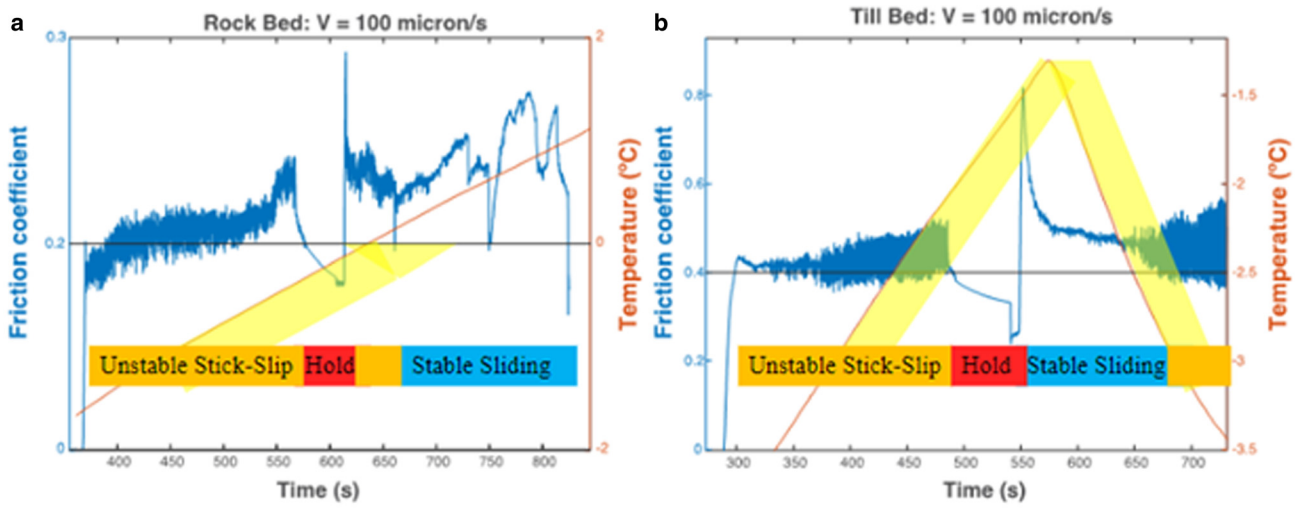

Figure 2. Example experiments of the temperature effect on slip stability for (a) rock and (b) till beds. Each experiment begins with stress-drops but, after a hold (described in section 2 above), with increasing temperature the ice starts to slide stably without sudden friction drops or audible stick-slips. The transition to stable sliding occurs ~ 0°C for the rock experiment. In the till experiment, the stability temperature is reached during the hold, but as it is re-cooled stress-drops do not resume until the temperature is below about −2.5°C. Each estimated transition temperature is highlighted with a thin black horizontal line, but temperature is not measured directly at the ice-bed interface, so the temperature at the interface lags that recorded. The lag time (estimated to be ~100 s) is represented by the yellow region right of the measured temperature. It is also apparent that the till experiment has a higher friction and healing rate (as the friction rose more after hold times of similar duration).

by the sum of the squared amplitudes of the first 400 sample points after the trigger, multiplied by a cosine taper (effectively weighting the earlier data points using a cosine shape, see Figure S2 in the supplement of Nolte and Pyrak-Nolte [2022]). Zero and large amplitude waveforms were removed, defined as having a sum of the first 400 normalized sample points greater than 15. This threshold was found to give the best catalog of non-noise events without greatly diminishing the catalog. 325 events were then removed that have high amplitude low frequency noise component. Finally, the waveforms were realigned to the first maximum peak after the trigger, which refined alignment by a few samples or less in most cases. From this catalog of normalized, filtered, and aligned 1200-sample point waveforms, we used a trial-and-error approach to determine how much of the pre- and post-trigger waveforms to use for training the models and found a total length of 150 sample points, with 45 before the trigger, was optimal, giving a 15-microsecond window. This subsample of the waveforms emphasizes the first arrivals of each AE, which are more dependent on source effects, while ignoring the coda (later wave arrivals), which depend more on path effects. Although the original, unprocessed catalog was able to produce as high prediction accuracies (supplementary text S2), not surprisingly since they contain more information, the processed waveforms were clearer to interpret, which is the main point of this study.

After removing noisy waveforms, we end up with 2817 total events, including 1547 waveforms from 6 till experiments and 1270 waveforms from 6 rock experiments, relatively balanced between bed types. With this labeled catalog (Fig. 3), we systematically explored the ability of numerous supervised classification ML algorithms to predict the bed type for each event based on their waveform and spectra. Classification ML models take a training dataset made up of feature vectors, each of which is labeled with a particular 'ground truth' class, and the model's parameters are optimized to predict the class of new, previously unseen feature vectors. In our case the features are the normalized amplitudes of each individual sample point in the event's AE waveform or log spectra, and the labels are the origin of the waveform, either a till or rock-bed. Each classification algorithm uses a different mathematical model to map the event to a specific class. Since our analysis focuses on results for the Random Forest Classifier model (Breiman, 2001) we briefly describe the underlying architecture of random forests.

A random forest is an ensemble learning model that incorporates the results of multiple decision trees. Each decision tree is a hierarchical, branching structure that splits a dataset into subgroups at each of several decision nodes based on the value of specific features. Random forests average the results of multiple trees, each of which is trained using a random sample of the data (bootstrap aggregating, or bagging) and a random sample of the feature space (feature bagging). This bagging procedure reduces overfitting the model on the training data. Since each decision is made based on a feature of the data, in this case the normalized amplitude at a certain time in the time series or power at a certain frequency in the spectrum of each event, we can inspect the tree to identify which parts of the waveform or which frequencies are most predictive. These 'feature importances' therefore allow us to interpret the model from a physical perspective.

In order to train and test the ML algorithms, we choose the most interpretable input features, the normalized waveform amplitudes at each time step or the $\log_{10}$ power at each frequency for the spectra, using the entire 15 microsecond time series. The waveforms and spectra were independently broken into train and test datasets and randomly assigned, containing 70 and 30% of the events, respectively. The trained models select the most important temporal portions of the waveforms or frequencies in the spectra for discriminating between bed labels. We tested a suite of six basic ML algorithms commonly used for classification problems. They are available with the scikit-learn python package (see Open Research section for github page with Jupyter notebook for all processing and analysis steps, as well as supplementary text S2 for more details). The algorithms we tested (and the mean prediction accuracy of each) are Naïve Bayes (~66%), XGBoost (~74%), support vector machines (~77%), random forests (~77%), fully connected neural networks (~75%) and K-nearest Neighbors (~75%). Hyperparameters were tuned for each algorithm and input data type (time or frequency domain) using 5-fold cross validation, and the highest-accuracy model for each algorithm was then used for prediction on the test set. The results of all our tests are summarized in supplementary text S2, but here we focus our analysis on the

https://doi.org/10.1017/aog.2024.11 Published online by Cambridge University Press

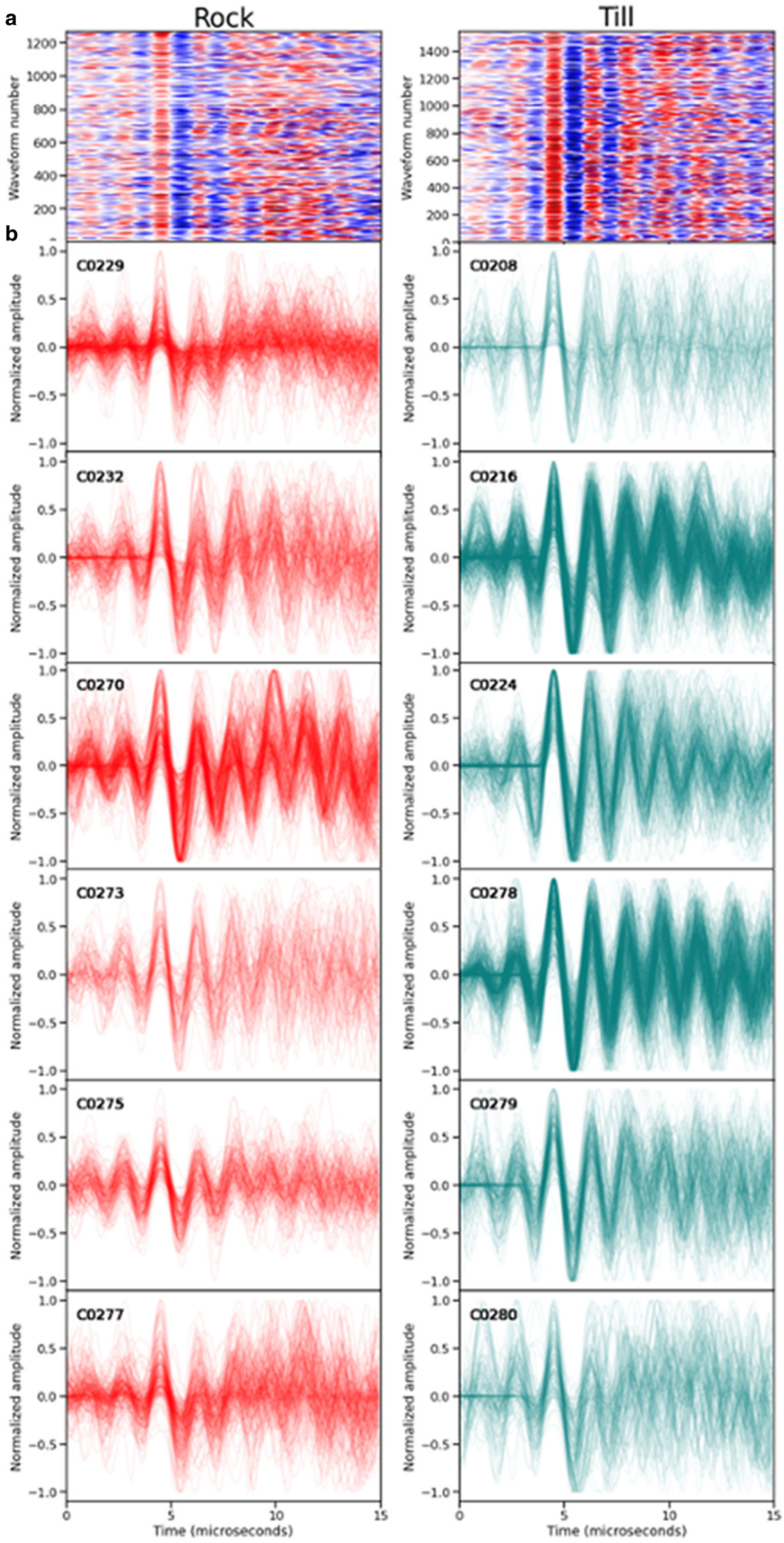

Figure 3. (a) Waveforms plotted in chronological order along *y*-axis, colored by (normalized) amplitude (red is positive and blue negative). Rock events are plotted on the left and till on the right. (b) Waveforms plotted together for each experiment (labeled on upper left). Sensors exhibit resonance, with waves at the resonant frequency present throughout the recording, even before the arrival, and thus should not affect the prediction. Each waveform (rock in red and till in teal) is plotted with a thin line, so the darker parts show many waveforms aligned on top of each other, and broader lines show less alignment. Since experiments vary significantly by number of events (94–465), that also contributes to the plot of each experiment's appearance. Number of events and bed temperature for each experiment, as well as experiment by experiment training and testing, in order to discount the possibility that experimental differences are being used in the prediction, are explored in supplementary text S3. Although there are subtle visual differences, it is not obvious that the two beds can be deciphered, making it a useful dataset to explore ML-based classification.

Random Forest Classifier model (Breiman, 2001) applied to the processed catalog, since it obtained some of our highest prediction accuracies, but, most importantly, the algorithm provides the feature importance needed to interpret how the model obtains its results. By showing the weighting of each waveform sample or frequency in making its prediction (Figs 4a and b), feature importance visually highlights the subtle differences between different event sources. The purpose of this study is to understand how bed differences manifest in the resulting emissions, not to find a black-box algorithm which best differentiates them.

https://doi.org/10.1017/aog.2024.11 Published online by Cambridge University Press

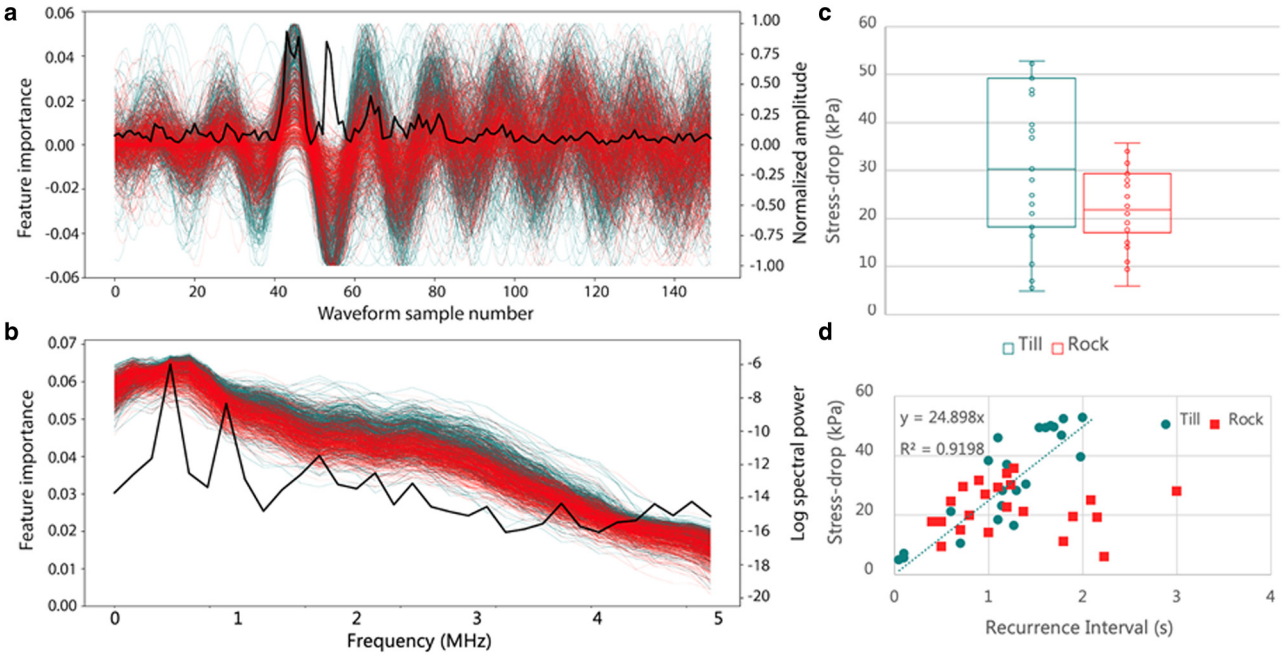

Figure 4. (a) Feature importance (black), showing the weighting of each waveform sample to the model prediction, highlights the importance of the initial, post-trigger, wave arrivals. The superimposed normalized waveforms show till (teal) events are higher amplitude than rock (red) in these first oscillations. (b) Feature importance (black) of each frequency in the model prediction, show till (teal) and rock (red) spectra partially separate from each other above about 1 MHz, with till having more energy at these higher frequencies. It is not clear why the model finds certain frequencies more important for prediction. (c) Distribution of largest repeated mechanical stress-drop amplitude from 23 till and 22 rock experiments at similar conditions show till has overall higher stress-drops, although the two populations overlap significantly. (d) Stress-drops vs recurrence interval for till and rock experiments shows till's greater healing (higher slope) contributes to higher stress-drops, while rock healing varies more, but is generally lower.

5. Bed type classification from acoustic emissions

Using a wide range of classification algorithms, we consistently find prediction accuracy above 50%, mostly between 65 and 80% (supplementary Figure S3), showing it is possible to tell if a population of AEs was emitted by a till or rock-bed. This is not clear by visually examining the waveforms (Fig. 3), so the algorithms successfully extract subtle waveform and spectral features corresponding to the different bed types.

To be able to apply our findings from laboratory AEs to field-scale seismicity, it is vital that we can interpret how the algorithms make their prediction. Although transfer learning methods offer the potential to train with labeled laboratory or modeled datasets and 'transfer' the model to more limited field or laboratory data (e.g., Wang and others, 2021), clear differences in the spectral content, travel path effects, and scale of field seismic data make this a difficult task. By isolating and interpreting the features the algorithms are using to make their successful

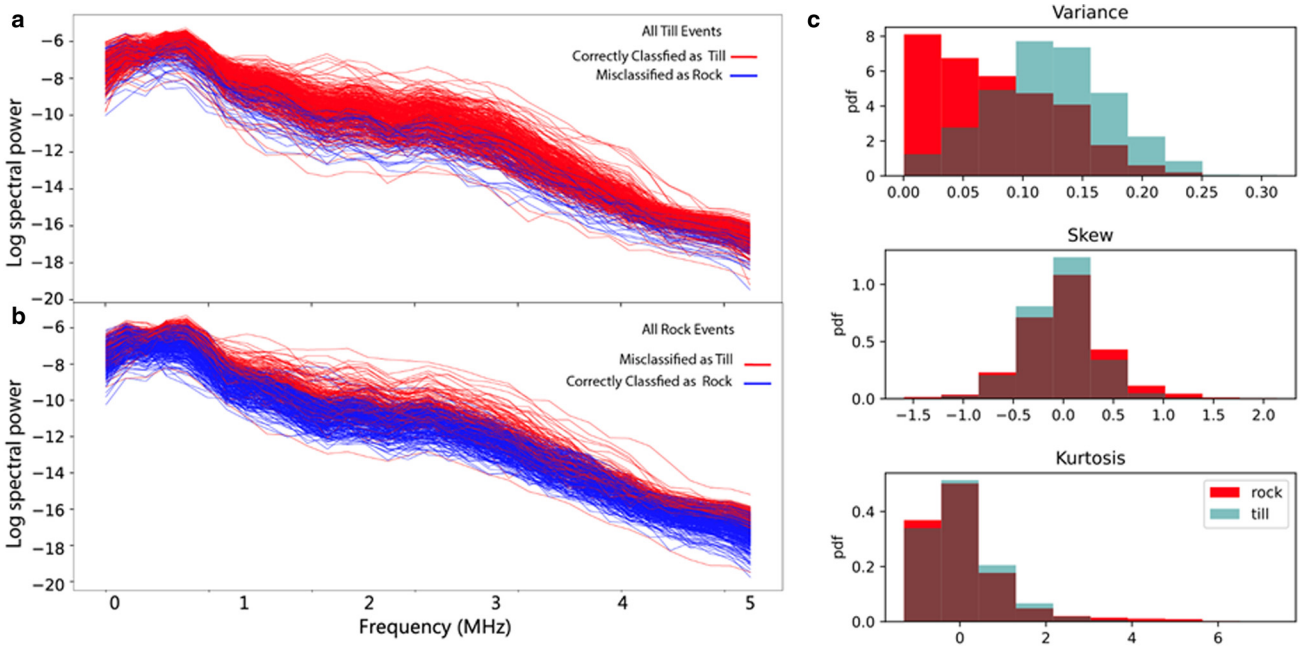

Figure 5. Log spectra of correct and misclassified (a) till and (b) rock events and (c) distributions of statistical measures of waveforms from all experiments from each bed show how much the event populations overlap. The higher variance in the till waveform distributions is due to their more impulsive nature, but there are many rock events with just as high variance.

https://doi.org/10.1017/aog.2024.11 Published online by Cambridge University Press

predictions, we can identify and quantify predictive features to closely examine for in field data. The feature importance for the Random Forest Classifier model shows that it focuses on the peak and valley of the first full oscillation of the initial wave arrival (Fig. 4a). Plotting all the normalized waveforms (color coded by bed type) together, we can see that the till (teal) waves tend to have higher amplitude in these first peaks. Similarly, log spectra show more energy at higher frequencies for the till in comparison to rock spectra (Fig. 4b). Analyzing the mechanical data from 23 till and 22 rock experiments (including experiments where AEs were not recorded), we find that the stress-drops of stick–slip events on till beds are generally higher (Fig. 4c). The more impulsive arrivals and higher frequency content is consistent with till's higher stress-drops, since seismological stress-drop is calculated by the corner frequency where energy starts to fall off (e.g., Zoet and others, 2012). This, in turn, can be explained by till's higher healing (Figs 2 and 4d), friction (Fig. 2), as well as the rougher till surface (with its larger grain sizes).

It is likely that obtaining much higher prediction accuracies is impossible given the similarity between waveforms. The stress-drop and healing rates of the two populations clearly overlap (Fig. 4c and d); spectra and waveform characteristics do as well. How these similarities affect prediction can be most clearly seen with the log spectra since the visual separation is clearest (Fig. 4b). Figure 5a and b show that misclassified events are in the region between the event types, while Figure 5c shows that the waveform statistical attributes also greatly overlap. Although correctly predicting every event is unrealistic, given a sufficient sample size, our results suggest it could be possible to predict the bed type of a group of events from the same source conditions (see supplementary text S4).

6. Conclusions

This study presents stick–slip stress-drops and resultant AEs for ice on rock and till beds at sub-freezing temperatures, a labeled dataset with which we explore how ML can decipher the bed from AE characteristics. We found that instability, and thus seismicity, only occurs for each bed below a certain temperature (~0° C for rock and ~−2.5°C for till), sliding stably as the temperature warms above and stick-slipping again when frozen below these temperatures, not precise due to limitations in our temperature measurement. Although the different bed types exhibit stick–slip behaviors at similar conditions, the mechanics of their drag are very different, demonstrated by friction that evolves over an order of magnitude more distance (D_c), significantly more rate-weakening ($b - a$), higher friction, and healing rates in frozen till compared to rock beds (Fig. 2 and Saltiel and others [2021]). Resultant emissions have subtle differences, difficult to decipher visually, but which ML-based classification was able to identify; successfully predicting the bed type of a given waveform about 65–80% of the time, depending on the classification algorithm, processing steps, and data type used. The Random Forest Classifier was particularly successful (~77% mean prediction accuracy) and interpretable, since it provides feature importance of each waveform sample or frequency, showing the models focus on the initial wave arrivals and certain frequencies where till events are higher amplitude. This is consistent with till's more impulsive failure, higher stress-drops, and friction, in turn due to a rougher and faster healing interface.

Given how different the slip mechanics of these two beds are, it is somewhat surprising how similar the resultant AEs are, but the interpretability of our ML results offers a path forward for classification. The findings are also counter to our original hypothesis based on the much longer frictional evolution distances (D_c) found in velocity-step experiments, which suggest less impulsive, lower frequency emissions. It is likely that different aspects of the frictional mechanics counter each other, for example more healing has been associated with higher frequency emissions in laboratory and natural faults (McLaskey and others, 2012), which could cancel out the spectral effect of longer D_c. In a similar way, till experiments' higher D_c and $b - a$ balance each other to produce a critical rheological stiffness (Eqn (1)) of the same order as rock (Saltiel and others, 2021). In the sense of a linear slip weakening law, the two beds would evolve with the same weakening slope, till friction just drops further over more distance, thus the stress-drops vary but the emission characteristics seem to be controlled by that slope and thus remain remarkably similar.

Our findings suggest that supervised ML-based classification and unsupervised correlation studies could find unknown and nonintuitive relationships between seismic emission characteristics and the mechanics/conditions of rupture in subglacial, as well as tectonic, volcanic, or induced seismicity settings. Laboratory experiments offer the opportunity to obtain well-controlled, labeled datasets, but results need to be interpretable. Although challenges remain for transferring models trained in the lab directly to field-scale data, the understanding gained though interpretable models can be used to infer characteristics of field-scale seismic sources.

Supplementary material. The supplementary material for this article can be found at https://doi.org/10.1017/aog.2024.11.

Acknowledgements. S. Saltiel acknowledges the support of the Lamont-Doherty Postdoctoral Fellowship in Earth and Environmental Sciences. This research and salary for S. Saltiel and C. McCarthy were funded by National Science Foundation NSF-1854629. T. Sawi was supported by NSF-GRFP-2036197. Many thanks to B. Holtzman and T. Mittal for data processing and ML analysis suggestions, J. Tielke and T. Koczynski for laboratory assistance, as well as C. Marone, J. Rivière, and the Penn State Rock and Sediment Mechanics Lab for experimental acoustics advice. We also acknowledge L. Zoet and A. Fowler for constructive reviews, which improved the manuscript.

Competing interest. None.

Open research. The datasets generated for this study are available on figshare.com at doi: 10.6084/m9.figshare.21257730, and Jupyter notebook for processing data is available at https://github.com/StraboAI/IcesAEs.

References

Aster RC and Winberry JP (2017) Glacial seismology. *Reports on Progress in Physics* **80**, 126801. doi: 10.1088/1361-6633/aa8473

Bougamont M and 5 others (2015) Reactivation of Kamb ice Stream tributaries triggers century-scale reorganization of Siple Coast ice flow in West Antarctica. *Geophysical Research Letters* **42**(20), 8471–8480.

Breiman L (2001) Random forests. *Machine Learning* **45**, 5–32. doi: 10.1023/A:1010933404324

Clarke GK (2005) Subglacial processes. *Annual Review of Earth and Planetary Sciences* **33**(1), 247–276.

Cuffey KM and Paterson WSB (2010) *The Physics of Glaciers*, 4th Edn. Burlington, MA, USA: Elsevier.

de Robin GQ (1976) Is the basal Ice of a temperate glacier at the pressure melting point? *Journal of Glaciology* **16**(74), 183–196. doi: 10.3189/S002214300003152X

Dieterich JH (1979) Modeling of rock friction: 1. Experimental results and constitutive equations. *Journal of Geophysical Research: Solid Earth* **84** (B5), 2161–2168.

Goldberg DN, Schoof C and Sergienko OV (2014) Stick-slip motion of an Antarctic ice stream: the effects of viscoelasticity. *Journal of Geophysical Research: Earth Surface* **119**(7), 1564–1580.

Gräff D and Walter F (2021) Changing friction at the base of an alpine glacier. *Scientific Reports* **11**, 10872. https://doi.org/10.1038/s41598-021-90176-9

Gräff D and 5 others (2021) Fine structure of microseismic glacial stick-slip. *Geophysical Research Letters* **48**, e2021GL096043. https://doi. org/10.1029/2021GL096043.

Guerin G, Mordret A, Rivet D, Lipovsky BP and Minchew BM (2021) Frictional origin of slip events of the Whillans Ice Stream, Antarctica. *Geophysical Research Letters* **48**(11), e2021GL092950.

Hudson TS and 7 others (2023) Highly variable friction and slip observed at Antarctic ice stream bed. *Nature Geoscience* **16**, 1–7.

Ida Y (1972) Cohesive force across the tip of a longitudinal-shear crack and Griffith's specific surface energy. *Journal of Geophysical Research* **77**(20), 3796–3805.

Iverson NR (2010) Shear resistance and continuity of subglacial till: hydrology rules. *Journal of Glaciology* **56**(200), 1104–1114. doi: 10.3189/002214311796406220

Kufner S-K and 5 others (2021) Not all icequakes are created equal: basal icequakes suggest diverse bed deformation mechanisms at Rutford ice stream, West Antarctica. *Journal of Geophysical Research: Earth Surface* **126**, e2020JF006001. doi: 10.1029/2020JF006001

Lipovsky BP and 6 others (2019) Glacier sliding, seismicity and sediment entrainment. *Annals of Glaciology* **60**(79), 182–192.

Lipovsky BP and Dunham EM (2016) Tremor during ice-stream stick slip. *The Cryosphere* **10**(1), 385–399.

Marone C (1998) Laboratory-derived friction laws and their application to seismic faulting. *Annual Review of Earth and Planetary Sciences* **26**(1), 643–696.

McCarthy C, Savage HM, Koczynski T and Nielson MA (2016) An apparatus to measure frictional, anelastic, and viscous behavior in ice at temperate and planetary conditions. *Review of Scientific Instruments* **87**(5), 055112.

McCarthy C, Savage HM and Nettles M (2017) Temperature dependence of ice-on-rock friction at realistic glacier conditions. *Philosophical Transactions of the Royal Society A* **375**(2086), 20150348.

McLaskey GC, Thomas AM, Glaser SD and Nadeau RM (2012) Fault healing promotes high-frequency earthquakes in laboratory experiments and on natural faults. *Nature* **491**(7422), 101–104.

Minchew BM and Meyer CR (2020) Dilation of subglacial sediment governs incipient surge motion in glaciers with deformable beds. *Proceedings of the Royal Society A* **476**(2238), 20200033.

Nolte DD and Pyrak-Nolte LJ (2022) Monitoring fracture saturation with internal seismic sources and twin neural networks. *Journal of Geophysical Research: Solid Earth* **127**(2), e2021JB023005.

Parizek BR and 10 others (2013) Dynamic (in) stability of Thwaites Glacier, West Antarctica. *Journal of Geophysical Research: Earth Surface* **118**(2), 638–655.

Rice JR, Lapusta N and Ranjith K (2001) Rate and state dependent friction and the stability of sliding between elastically deformable solids. *Journal of the Mechanics and Physics of Solids* **49**(9), 1865–1898.

Ruina A (1983) Slip instability and state variable friction laws. *Journal of Geophysical Research: Solid Earth* **88**(B12), 10359–10370.

Saltiel S, McCarthy C, Creyts TT and Savage HM (2021) Experimental evidence of velocity-weakening friction during ice slip over frozen till: implications for basal seismicity in fast moving, soft-bed glaciers and ice streams. *Seismological Research Letters* **92**(5), 2793–2810.

Schulson EM and Fortt AL (2012) Friction of ice on ice. *Journal of Geophysical Research: Solid Earth* **117**(B12).

Sergienko OV, MacAyeal DR and Bindschadler RA (2009) Stick–slip behavior of ice streams: modeling investigations. *Annals of Glaciology* **50**(52), 87–94.

Stevens NT and 6 others (2024) Icequake insights on transient glacier slip mechanics near channelized subglacial drainage. *Earth and Planetary Science Letters* **627**, 118513.

Thøgersen K, Gilbert A, Schuler TV and Malthe-Sørenssen A (2019) Rate-and-state friction explains glacier surge propagation. *Nature Communications* **10**(1), 2823.

Thomason JF and Iverson NR (2008) A laboratory study of particle ploughing and pore-pressure feedback: a velocity-weakening mechanism for soft glacier beds. *Journal of Glaciology* **54**(184), 169–181.

Wang K, Johnson CW, Bennett KC and Johnson PA (2021) Predicting fault slip via transfer learning. *Nature Communications* **12**(1), 1–11. doi: 10.1038/s41467-021-27553-5

Weertman J (1957) On the sliding of glaciers. *Journal of Glaciology* **3**(21), 33–38.

Zoet LK and Iverson NR (2016) Rate-weakening drag during glacier sliding. *Journal of Geophysical Research: Earth Surface* **121**(7), 1206–1217.

Zoet LK and Iverson NR (2020) A slip law for glaciers on deformable beds. *Science* **368**(6486), 76–78.

Zoet LK, Anandakrishnan S, Alley RB, Nyblade AA and Wiens DA (2012) Motion of an Antarctic glacier by repeated tidally modulated earthquakes. *Nature Geoscience* **5**, 623–626.

Zoet LK and 6 others (2013) The effects of entrained debris on the basal sliding stability of a glacier. *Journal of Geophysical Research: Earth Surface* **118**, 656–666.

Zoet LK and 6 others (2020) Application of constitutive friction laws to glacier seismicity. *Geophysical Research Letters* **47**(21), e2020GL088964.

https://doi.org/10.1017/aog.2024.11 Published online by Cambridge University Press